Aeolian Research, 2016 (accepted) http://dx.doi.org/10.1016/j.aeolia.2016.09.003

Evaporative sodium salt crust development and its wind tunnel derived transport dynamics under variable climatic conditions

Joanna M. Nield[1,*], Cheryl McKenna Neuman[2], Patrick O'Brien[2], Robert G. Bryant[3], Giles F.S. Wiggs[4]

[*]Corresponding author: Email: J.Nield@soton.ac.uk; Tel: +44 23 8059 4749

[1] Geography and Environment, University of Southampton, Highfield, Southampton, UK, SO171BJ

[2] Department of Geography, Trent University, Peterborough, ON, Canada K9J 7B8

[3] Department of Geography, University of Sheffield, Sheffield, S10 2TN, UK

[4] School of Geography and the Environment, Oxford University Centre for the Environment, University of Oxford, Oxford, OX1 3QY, UK

Abstract

Playas (or ephemeral lakes) can be significant sources of dust, but they are typically covered by salt crusts of variable mineralogy and these introduce uncertainty into dust emission predictions. Despite the importance of crust mineralogy to emission potential, little is known about (i) the effect of short-term changes in temperature and relative humidity on the erodibility of these crusts, and (ii) the influence of crust degradation and mineralogy on wind speed threshold for dust emission. Our understanding of systems where emission is not driven by impacts from saltators is particularly poor. This paper describes a wind tunnel study in which dust emission in the absence of saltating particles was measured for a suite of climatic conditions and salt crust types commonly found on Sua Pan, Botswana. The crusts were found to be non-emissive under climate conditions characteristic of dawn and early morning, as compared to hot and dry daytime conditions when the wind speed threshold for dust emission appears to be highly variable, depending upon salt crust physicochemistry. Significantly, sodium sulphate rich crusts were found to be more emissive than crusts formed from sodium chloride, while degraded versions of both crusts had a lower emission threshold than fresh, continuous crusts. The results from this study are in agreement with in-situ field measurements and confirm that dust emission from salt crusted surfaces can occur without saltation, although the vertical fluxes are orders of magnitude lower (~ 10 $\mu g/m/s^1$) than for aeolian systems where entrainment is driven by particle impact.

Key Words: sodium sulphate (mirabilite and thenardite); sodium chloride (halite); aeolian dust source; playa; surface crust; wind tunnel

1. Introduction

Playas (or ephemeral lakes) contain vast reserves of silt and clay which, periodically, can become susceptible to erosion by wind; and thus are considered to be major dust sources on a global scale (Gill, 1996; Baddock et al., 2009; 2016; Bullard et al., 2011; Prospero et al., 2002; Washington et al., 2003; 2006). Some proportion of these dry lake beds is usually either protected by an evaporitic salt crust that substantially reduces dust emission (Baddock et al., 2011; Houser and Nickling, 2001; King et al., 2011; Nickling and Ecclestone, 1981; Nickling, 1984; O'Brien and McKenna Neuman, 2012; Sweeney et al., 2011; Webb and Strong, 2011), or have surfaces that are moist or temporarily flooded (e.g. Mahowald et al., 2003; Bryant et al., 2007; Hahnenberger and Nicoll, 2014; Nield et

al., 2016). Crusted playa surfaces are morphologically and geochemically dynamic and can respond rapidly to changes in the local environmental conditions (Figure 1a; Gillette et al., 2001). During periods with standing water (e.g. following heavy rain), the playa surface resets to form an expansive featureless plain; a physical crust end-member that, in the context of the present paper, will be described as 'continuous' (Figure 1b; Nield *et al.*, 2015). With crust development and expansion (typically through mineral precipitation), these surfaces can develop a 'ridged' topography that, in response to horizontal pressure equalisation, often has a plan-form characterised by a series of interconnected polygons. Over time, the continued operation of both mechanical and chemical processes acting on the playa surface ultimately leads to decay of the salt crust integrity to a point where it can be categorized as having a friable or 'degraded' physical state (Figure 1c; Gillette et al., 2001; Reynolds et al, 2007; Nield et al., 2015). Degraded crusts often exhibit small-scale roughness (mm) but have limited meso-scale topography (mm – cm; Nield et al., 2015; 2016). However, degraded crusts typically protect an underlying 'fluffy' layer of sediment (1-5 cm thick) which represents salty sediment of dust-size fraction with notably low bulk density that is readily eroded by wind (Nield et al., 2015; Reynolds et al., 2007), particularly if the crust has been disturbed or broken due to animal activity, saltation or vehicular traffic (e.g. Gillette et al., 2001; Baddock *et al.,* 2011).

In-situ measurements of dust emission (e.g. Cahill et al., 1996; Gillette et al., 2004; King et al., 2011; Sweeney et al., 2011; 2016) and evaporation on playas (e.g. Groeneveld et al., 2010; Kempf and Tyler, 2006; Tyler et al., 1997) exhibit a large degree of variability that is directly attributed to the crust type (e.g. continuous, ridged or degraded), condition (e.g. undisturbed or disturbed) and chemistry (e.g. Buck et al., 2011; Tollerud and Fantle, 2014; Haustein et al., 2015; Sweeney et al., 2016). Over large playas, the heterogeneity of the crust (Kempf and Tyler, 2006; Nield *et al.,* 2013) significantly increases the uncertainty of predictive dust emission models (Bryant, 2013). Whilst field studies of the interplay between crust type, salt concentration and environmental conditions are urgently needed, it is extraordinarily difficult to manipulate each physical attribute systematically and monitor the associated dust emission with a high level of precision. Previous wind tunnel studies have investigated particle entrainment from coarse granular surfaces (sand) sprayed with a NaCl solution of varied concentration to form brittle crusts having a range of yield strength (Langston and McKenna Neuman, 2005; Nickling and Ecclestone, 1981; Nickling, 1984; O'Brien and McKenna Neuman, 2012). While the described methodologies are directly transferrable to the investigation of dust emission from playas, the construction of crusts through salt spray does not accurately recreate the physical characteristics below the surface (top mm) of in-situ crusts. Salt pans and the crusts that form there are typically produced through evaporation of pore water from fine-grained sediments (silt and clay). Thus, it remains unclear how the physicochemical characteristics unique to this particular geophysical setting govern dust emission.

Salt chemistry plays a key role in crust development. However, evaporative responses are complex and depend on the grain size of the surface sediment, salt concentration, moisture (groundwater depth) and temperature/relative humidity (Nachshon *et al.,* 2011a; Nachshon *et al.,* 2011b; Rad *et al.,* 2013). For example, sediment porosity controls moisture transfer through capillarity (Tyler *et al.,* 1997). In the case of fine sediment, salt efflorescence (or sub-efflorescence) facilitates crust formation and thereby reduces evaporation, whilst coarse sediment typically develops patchy salt efflorescence with increased evaporation rates (Eloukabi *et al.,* 2013). Likewise, salt chemistry can alter the dust emission potential of a surface, with sodium sulphate (Na_2SO_4) salts being associated with particularly emissive surfaces (Buck et al., 2011; King et al., 2011; Reynolds et al., 2007) and a common component of many global playas (Langbein, 1961; Rosen, 1994). In this instance, sodium sulphate is particularly sensitive to changes in ambient environmental conditions and can switch between hydrated mirabilite ($Na_2SO_4 \cdot 10H_2O$) and dehydrated thenardite (Na_2SO_4). Mirabilite typically forms when the relative humidity is above 60 - 75% for temperatures between 0°C and 20°C (Kracek, 1928; Steiger and Asmussen, 2008). This occurs through the dissolution of thenardite and the subsequent recrystallisation of mirabilite (Thaulow and Sahu, 2004), which may

increase the size of the salt crystals significantly; often by fourfold or more (Saint-Amand *et al.,* 1986; Tsui *et al.,* 2003). Sodium chloride (NaCl; halite) is also a key component of many dust emitting playas (Langbein, 1961; Rosen, 1994). Although NaCl is less responsive to changes in temperature (Benavente *et al.,* 2015), NaCl has the ability to modulate the phase change of Na_2SO_4 and thereby alter the apparent dust emission potential of surfaces that contain multiple Na-phases (Buck *et al.,* 2011). Whilst laboratory and in-situ studies have substantially advanced our understanding of salt-related damage in built environments caused by sodium salts for a range of environmental conditions (Genkinger and Putnis, 2007; Rodriguez-Navarro et al., 2000; Shahidzadeh-Bonn et al., 2010; Tsui et al., 2003; Viles and Goudie, 2007), much research remains to be carried out regarding reactions that occur in porous materials/sediments found on playas (Espinosa-Marzal and Scherer, 2010).

In this paper we report on a series of experiments which directly address some aspects of this paucity of data. The experiments were carried out in a wind tunnel in which the temperature, humidity and wind speed were precisely controlled over specified periods of time. Whilst we did not specifically monitor salt crystal geochemistry, temperature, relative humidity and initial Na_2SO_4 concentrations followed known sulphate phase transitions between thenardite and mirabilite (Kracek, 1928; Steiger and Asmussen, 2008). The meteorological conditions within the tunnel simulated those of a known emissive dust source (Sua Pan, Botswana) during the dry, dusty winter period (Haustein et al., 2015; Nield et al., 2015; Nield et al., 2013; Vickery, 2014). Sua Pan is part of the Makgadikgadi Pans and a major source of suspended dust in the Southern Hemisphere, particularly during winter months (Prospero *et al.,* 2002; Washington *et al.,* 2003; Zender and Kwon, 2005). Based upon extensive field studies during the Dust Observations for Models (DO4) campaign in 2011 and 2012, two physical end-member crust examples (continuous and degraded; e.g. Nield et al., 2015; 2016), along with common salt chemistries observed on the Sua Pan (Eckardt *et al.,* 2008), were studied in order to evaluate the:

i) Morphological development of surface crusts when exposed to diurnal cycles of temperature and relative humidity in the context of controlled variation in the evaporation rate;

ii) Susceptibility to wind erosion/dust emission of the crusts under climatic conditions associated with arid-climates at key stages in the diurnal cycle: (a) dawn, (b) mid-morning, and (c) mid-day; and

iii) Change in the threshold wind velocity for dust emission after the crust structure had been disturbed.

2. Methods

2.1. Crust Preparation

Nineteen crusts replicating physical continuous and degraded playa surfaces were prepared from mixtures of sediment and salt water using varied treatments described below. Symbols and numbers are used to identify these crust types using the notation explained in Table 1. As an initial basis for experimentation, two crust samples were formed by adding distilled water to sediment collected directly from the surface of Sua Pan, Botswana (20.5754°S, 25.959°E); thus re-mobilising the salts. Quartz is the primary mineral comprising the silt and clay sized particles contained in this sediment. Only a small sample of Sua Pan sediment was available for testing. Consequently, the remaining 17 experimental crusts were formed using ground nepheline syenite (predominantly, and referred to subsequently, as feldspar) that was milled at a site near the laboratory facility and

selected on the basis that it had a similar grain size distribution and particle density to the pre-treatment Sua Pan sediments (Figure 2; mean grain size for playa and feldspar: 33 μm and 42 μm respectively). The ground feldspar also had the advantage that it was plentiful in supply and non-toxic when inhaled. Thereafter, salt solutions containing different concentrations of either Na_2SO_4, NaCl or a mixture of both were applied to the 'rock flour' base material by initially dissolving specific salt crystals in warm distilled water so as to form saturated solutions for each salt (26.4 wt % halite, 35 wt % and 16.5 wt sodium sulphate representing the saturation concentrations of thenardite and mirabilite respectively, given the typical temperature and relative humidity conditions that these dehydrated and hydrated salts precipitate out at (Shahidzadeh-Bonn *et al.*, 2010)). The solutions were then combined carefully to produce 9 different mixture concentrations (Table 1), representative of the chemistry typical of Sua Pan, Botswana (Vickery, 2014) and common on other dust emitting playas (e.g. Bryant et al., 1994; Gillette et al., 2001; Reynolds et al., 2007; Buck et al., 2011; Sweeney et al, 2016).

Each test surface was contained within a small 26 x16 cm aluminium tray that was suitable for transport by hand and placement into the floor of the wind tunnel. From previous experience in the facility, it is known that large surfaces fracture easily with even the slightest flexure of the container in which they are formed. The bottom of each pan was lined with a 1 cm thick layer of stiff, 'humidifier' foam that was covered with Nytex™ mesh in order to prevent vertical seepage of the overlying feldspar particles. With the addition of a fixed volume (220 ml) of a given salt solution to the base of each tray, the highly porous foam acted as an effective moisture reservoir that mimicked the surface conditions observed on playas (Vickery, 2014) in allowing the upward movement of water by capillarity in compensation for evaporative losses from the surface. Importantly, the experimental design allowed the within-pore (sub-surface) structure to form concurrently with efflorescent (surface) crusts.

Three separate treatments were adopted in preparing a given crust. The simplest of the three (Treatment 1) involved pouring dry, loose feldspar particles into each tray, levelling them, and then spraying a salt solution evenly over the surface with a pressurized paint sprayer, similar to the methodology carried out by Langston and McKenna Neuman (2005) and O'Brien and McKenna Neuman (2012). For the remaining trays (treatments 2 and 3), a small quantity of the respective salt solution was added to the oven dried sediment and hand-mixed to a consistent 'bread-crumb' type texture with 17% mean gravimetric moisture content (minimum 16%, maximum 19%), similar to the moisture content of sediment in contact with the crust on Sua Pan. For Treatment 2, this moist sediment was then placed in the tray overtop of the foam reservoir and vibrated until it formed a smooth, wet surface level with the top edge of the tray. Alternatively, for Treatment 3, moist sediment was added initially, vibrated until it assumed a flat profile in tight contact with the Nytex mesh, and then topped up with the remainder of the moist sample having a 'bread crumb' texture that mimicked the low density structure of natural degraded playa surfaces.

Following their preparation, all trays were placed in a climate controlled chamber for two weeks and exposed to diurnal cycles of temperature (T) and relative humidity (RH) alternating between warm ($20°C \leq T \leq 25°C$) and dry ($30\% \leq RH \leq 40\%$), or cool (11°C) and humid (RH= 60%) conditions, similar to the mean day time and night time conditions recorded at Sua Pan, Botswana during August and September 2012 (the typical dust season). These meteorological conditions were also chosen to induce a switch in the Na_2SO_4 phase from mirabilite in the cool conditions to thenardite in the warm and hot conditions (Kracek, 1928; Steiger and Asmussen, 2008).

At the time of each change in T and RH (e.g. twice daily: day and night), each tray was weighed to determine the evaporation rate over the preceding 12 h period. The crust topography then was scanned in 10 x 20 cm sections using a Konica-Minolta Vivid9i 3-D laser scanner in order to determine any change in volume. The laser scanner had a vertical change detection resolution between 0 and 0.1 mm (O'Brien and McKenna Neuman, 2012). Crust elevation points were

gridded at 0.1 mm spacing and empty cells were interpolated in Matlab (Mathworks Inc) using the natural neighbour method. Elevation change ratios were calculated between each scan as the ratio of surface contraction (negative change) and expansion (positive change). Low ratios correspond to increased crystal development or surface expansion; high ratios signify slow crystal development or dissolution of crystal leading to surface contraction. Surface moisture and salt crystal development were inferred using a LTL Acorn 5211A time-lapse camera with an infra-red flash at 940 nm. The camera was placed 1.45 m above the crust samples and recorded images every five minutes with a resolution of 5 mega pixels. Digital numbers (DN) within the centre of each crust sample tray (150 x 50 pixels) were normalised using the average DN within a calibration white board. A low ratio value corresponds to greater absorption of the infra-red light source and is suggestive of high surface moisture content or low amounts of salt crystal on the surface (Mees *et al.,* 2011; Nachshon *et al.,* 2011a).

2.2. Wind tunnel measurement of dust emission threshold

The wind tunnel experiments for this study were carried out in an open circulation, suction type facility at Trent University. Details concerning the facility have been described in numerous early publications (e.g. McKenna Neuman 1998; Nickling and McKenna Neuman 1997) and are available online (http://people.trentu.ca/cmckneuman/website/facilities.html). The dimensions of the tunnel working section are listed as follows: height (Z) 0.74 m, width (Y) 0.71 m, and length (X) 13.5 m, giving a cross-sectional area of 0.54 m^2. The velocity in the freestream (u_∞) at z_∞ = 0.35 m is varied by adjusting the fan rpm, and can be held to within 2% of the 10 minute mean velocity. The length to height ratio of 18.2 well exceeds the minimum value of 5 suggested by White and Mounla (1991) for the natural development of a boundary layer. Large scale turbulent eddies generated by objects in the surrounding room are eliminated by flow-straightening tubes at the inlet to the compression bell. The boundary layer reaches its full thickness (δ) of 0.25-0.30 m at a distance approximately 2.5 meters downwind of a trip plate at the tunnel entrance. Wind velocity is sampled using a Dwyer micro-pitot tube (1 mm ID) that traverses vertically through the boundary layer on a microprocessor controlled slide (McKenna Neuman, 2003; McKenna Neuman, 2004). As is standard practice in aeolian transport studies, shear velocity (u*) was determined by fitting the Prandtl equation

$$u_z = \frac{1}{k} u_* \, ln\left(\frac{z}{z_o}\right) \quad (1)$$

to measurements of wind speed (u_z) from vertical profiles, where z is the vertical distance from the surface (m), z_o is the roughness length (7x10^{-6} m for the present tests, measured upwind of the crust samples), u_* is the shear velocity (m/s) and k is von Karman's constant. The entire wind tunnel is housed in an environmental chamber with full temperature (± 0.5 °C) and humidity (± 1 %) control.

The experiments described herein were undertaken using three different temperature and humidity settings based directly on the environmental conditions measured on the surface of Sua Pan, Botswana during the dry, dusty season in August and September 2012. Climate data were recorded every ten minutes at 1 m above the surface of Sua Pan (site location centred around 20.5754°S, 25.959°E) using CS215 (Campbell Scientific, Inc) temperature and relative humidity probes, housed in a radiation shield. The first three experiments (A-C) were undertaken on undisturbed crust samples. Additional tests using disturbed (D) or uncrusted sediment were also undertaken for some of these climate settings. The climate conditions used in each wind tunnel experiment are listed as follows,

A) The 'cold' or 'dawn' condition of 11.5°C and 54% relative humidity was based on mean measured Sua Pan values (n = 732) between 5 and 7 am (approximate sunrise); undisturbed crusts.

B) The 'warm', or 'morning' condition of 21.5°C and 37% relative humidity was based on mean measured Sua Pan values (n = 732) between 8 and 10 am (approximate time dust devils typically become visible on the playa); undisturbed crusts.
C) The 'hot' or 'daytime' condition of 29°C and 23% relative humidity was based on mean measured Sua Pan values (n = 732) between 11 am and 1 pm; undisturbed crusts.
D) Disturbed crusts using the same temperature and relative humidity conditions of C.

An un-crusted control sample using oven dried, untreated base-sediment without any additional moisture was tested under each environmental condition (A-C), and two additional uncrusted samples were tested for condition C (hot, daytime): 1) Sua sediment and 2) feldspar sediment that had been treated with salt water and then oven dried.

Only select samples of the most friable crusts were tested under conditions A and B (Table 1). Additional tests (condition D) determined the change in dust emission threshold between C and D, after the crust samples were disturbed by punching ~6 mm diameter holes through the crust to expose the low density, 'fluffy' sediment underneath (or untreated sediment in the spray crust examples).

Prior to loading each crust sample into the tunnel, all potential alternate sources of dust-sized material in the lab were either removed or covered, and all lab surfaces were carefully cleaned and wiped down with a damp cloth. Each crust was then lowered into a cut-out in the wind tunnel floor that was of a similar size to the tray, so that the top of the crust was aligned with the surrounding floor plates in the wind tunnel floor (Figure 3). The surrounding floor plates consisted of plywood coated with carpenter's glue and 150 mm sand, approximating the z_o of the crust samples. Each crust sample was oriented with its long axis (26 cm) parallel to the flow direction, approximately 11 m downwind of the tunnel entrance. In the spanwise direction (perpendicular to the flow), the crust sample was located in the centre of the working section, equidistant from the walls.

For all experiments, any emitted dust was monitored continuously using two non-isokinetic TSI DustTrak™ aerosol monitors (model 8250, precision 1 μg/m^3) while the freestream velocity (u_∞, measured immediately upwind of the crust sample) was stepped up from a starting velocity of 4 m/s in 0.25 m/s increments every 30 seconds up to 9.5 m/s for conditions A and B, and 14 m/s for conditions C and D. PM_{10} (aerodynamic diameter ≤ 10 μm) concentrations were sampled at a rate of 1 Hz and averaged over a 5 s period in order to synchronize with the wind velocity measurements. The DustTraks were mounted in a vertical array (z_1= 0.025 m and z_2 = 0.25 m) immediately downwind of the test surface. The upper DustTrak (z_2) reading is strongly indicative of the reference PM_{10} concentration of the intake air into the tunnel working section, as compared to that at z_1 which detects the additional dust loading associated with emissions directly from the test surface. The difference between the two readings (c_1-c_2) can then be used to determine the vertical dust flux (F; μg/m^2/s^1) as obtained from the following equation:

$$F = \frac{-ku_* (c_1 - c_2)}{\ln(\frac{z_2}{z_1})} \qquad (2)$$

Ambient dust levels in the lab were observed to rise slightly as the fan speed was increased, suggesting either some recirculation of emitted dust back to the wind tunnel inlet, and/or re-suspension of fine particulates within the lab. Sampling the PM_{10} concentration (c) at z_2 thereby provides a means of effectively correcting for this effect. The threshold for dust emission was determined in the present study when the maximum recorded value for c_1-c_2 exceeded 100 μg/m^3 for two consecutive sampling periods (Figure 4).

Finally, crust samples were weighed before and after each experiment to determine total mass loss and the surface elevation change over a sub-section (0.07 x 0.12 m) was measured again using the 3-D Konica-Minolta Vivid 9i scanner.

3. Results and Discussion

3.1. Salt crust development

Overall, the laboratory-derived salt crust samples developed characteristics that were morphologically similar (Figure 5) to the field examples (Figure 1) with regard to crust thickness, micro-topography and the presence of a low density sublayer. In general, salt efflorescence took several days to appear on the crust surfaces and continued to increase in coverage over time (Figure 6). The rate of crystal development was greatest during the hot, dry (daytime) phases, as indicated by an increased DN ratio on the surface (Figure 7).

Evaporation rates varied as the salt crusts developed, and were principally governed by the crust type and the salt concentration. In agreement with the small-scale findings of Eloukabi et al. (2013), Treatment 2 resulted in rapid formation of a uniform (continuous) crust that acted to reduce the evaporation rate over time. The playa-derived sediment also quickly formed a continuous crust which almost eliminated evaporation over time; as for example, after one week of development, evaporation rates for P2 were < 2% of the evaporation rate on the degraded crust (P3). In comparison, degraded crusts with low salt concentrations also had higher evaporation rates than either the continuous or degraded salt-rich crusts. There are at least three possible explanations for the observed changes in evaporation rates: 1) that the finer porosity in the continuous crust likely enhanced salt precipitation which accelerated crust formation and thereby reduced evaporation through occlusion of surface pores (Rad *et al.,* 2013), 2) that the patchy efflorescence on the degraded crust likely maintained evaporation rates over a longer period as the crust offered incomplete coverage of pores (Eloukabi *et al.,* 2013) and 3) that the greater porosity of the degraded crust likely increased sample heterogeneity and enabled sub-efflorescence to occur within pores (below surface) deeper in the sample (Nachshon *et al.,* 2011b).

Observed variation in the elevation of the continuous and degraded surfaces does not show a clear relationship with respect to either the method of preparation (treatments 1-3), or the type or amount of salt applied. Rather, the response appears to be controlled more by a combination of temperature regime and development time (Figure 8); with higher temperatures encouraging more salt crystal development either though efflorescence or sub-efflorescence. Similar surface elevation increases were observed by Nachshon et al. (2011a) and ascribed to evaporation and sub-surface salt precipitation. These researchers observed that crystal growth may displace existing crystals/matrix material by more than 1.5 mm. Interestingly, the laser scans obtained in the present study confirm that some of the low temperature surfaces showed a shift in crystal position and increased crystal growth in isolated regions (maximum change was 0.6 mm), despite a general decrease in elevation (mean and minimum changes were -0.4 mm and -1 mm, respectively) over the entire crust sample (Figure 8c). Nevertheless, crystal growth was in general greatest at higher temperatures (low elevation ratio; maximum, mean and minimum elevation changes were 3.6 mm, 1.5 mm and 0.0 mm, respectively; Figure 8d). Increased crystal growth can act as a sediment supply (Gillette et al., 2001) and previous field studies have noted the potential importance of fluctuating temperature and relative humidity in developing friable, dust emitting surfaces (Reynolds et al, 2007; Buck et al., 2011).

3.2. Dust emission threshold and vertical flux

In evaluating the relative importance of the physical and chemical characteristics of the various crusts tested here with regard to their capability to generate fine dust, the threshold shear velocity (u_{*t}) provides a useful index of the constraints on the relative particle supply from samples. Notably, we observed that the crusts tested under dawn and early morning conditions (A and B) did not emit any dust for free stream wind speeds at or below 9.5 m/s ($u_* \leq 0.38$ m/s). Under the warmer, drier conditions typical of daytime (condition C), however, all crusts emitted measureable dust, with the exception of one crust comprised of a low concentration of mixed salt that was degraded (M3[3.3,21.1]$_C$). As shown in Figure 9, threshold shear velocities (u_{*t}) varied from

0.26 m/s for a degraded Na_2SO_4 crust (T3[35]$_C$) and the uncrusted Sua Playa sediment (P4$_C$), up to 0.56 m/s for various crusts (continuous –M2[7,21.1]$_C$; degraded- M3[2,12]$_C$ and H3[15]$_C$). Significantly, these values, as measured in the wind tunnel with simulated crusts, fall within a similar range of threshold values measured in-situ (0.2 – 0.85 m/s) at Sua Pan, Botswana (Haustein *et al.,* 2015). The varied response among the different crust treatments was also found to be in agreement with field measurements at the Salton Sea, where Buck et al. (2011) observed that degraded Na_2SO_4 crusts (e.g. T3[35]$_C$) were more emissive than the predominantly smooth, well cemented halite-rich crusts (i.e. similar to M2[7,21.1]$_C$ in this study). In the current study, the T3[35]$_C$ crust was particularly efflorescent, bearing a soft, powder-like surface texture that has been associated with high dust emission rates (e.g. on the order of 10 to 100 $\mu g/m^2/s^1$) from similar salt crusts observed in field studies in the absence of impacts from saltating sand particles (Gillette *et al.,* 2001; King *et al.,* 2011; Sweeney *et al.,* 2011).

Mechanical rupture (hole punching) of the experimental crusts typically reduced u_{*t} for day time conditions by an average of 15.6% for all crust types, 23.2% for the degraded crust group (Figure 9c), and by as much as 50% for M1[7,21.1]$_D$, a crust formed from spraying mixed salt onto the surface. As a general rule, thinner crusts were also found to have a lower threshold wind speed for dust entrainment than thicker crusts (Pearson's linear correlation coefficient 0.72; Figure 10a), with P2 forming the thinnest crust (0.25 mm) and H3[26.4] the thickest (12 mm). However, once the experimental crusts were ruptured, their thickness had less influence on u_{*t} (correlation coefficient 0.1; Figure 10c).

The vertical PM_{10} flux was calculated for each concentration difference (c_2-c_1) sampled, following Equation 2. The average flux value from each experiment carried out over an undisturbed crust is in the order of 1 $\mu g/m^2/s^1$ (Table 2). The small area of the test bed, the severe limitation on the supply of dust available on the surface, and the absence of particle impact (saltation) are all factors which contribute to these low amounts of emission. Crust disturbance (condition D), in comparison, lead to highly variable increases in the proportionate amount of dust emitted (4% < F_D/F_C <95%; mean increase 52%) as compared to the original (i.e. undisturbed; condition C) crust in each case. The largest amounts of dust emitted (as high as 100 $\mu g/m^2/s$) were associated with the uncrusted playa sediment (P4$_C$), the degraded Na_2SO_4 crust (T3[35]$_C$), and the crushed feldspar (M4[7,21.1]$_C$ and W4$_C$ uncrusted), all of which were one to two orders of magnitude higher than those values for the remaining tests. To provide a meaningful context, the range in magnitude of these low vertical flux values falls within that measured in the field during dust emission events on Sua Pan (1 – 1000 $\mu g/m^2/s$) in 2011 (Haustein *et al.,* 2015). Macpherson et al. (2008) did not find any noticeable increase in dust emission rates between disturbed and undisturbed crust which they attribute to the strength of the salt cohesive bonds (Nickling and Ecclestone, 1981). It is likely salt bonding also influenced the variability in response between our samples and more investigations into the geochemistry influence are required (Buck et al., 2011).

When the fluxes for each experiment were plotted as a function of the respective shear velocity (Figure 11), several tests show a significant degree of correlation as reported in Table 2. These include, for example, all of the uncrusted surfaces, several playa crusts (Treatment 2 – disturbed and undisturbed), and various crushed feldspar crusts. Exponents in the power law relation

$$F = a\left(\frac{u_*}{u_{*t}}\right)^b \qquad (3)$$

average b ~ 4 for the relationships shown to be significant ($p<0.01$ and $r^2>0.5$). However, these values demonstrate substantial divergence from test to test, with the uncrusted surfaces being higher at approximately 6 and some durable crusts having exponents as low as 1. Such values lie within the range of those reported in the literature for both field and lab studies (e.g. between 1 and 7 see Table 1 in Sanderson *et al*, 2014).

3.3. Mass loss

Mass loss from the experimental surfaces may be attributed to any or all of the following processes: i) creep and saltation of aggregates loosened from the ruptured crust that are too heavy to enter into suspension, ii) increased evaporation with near surface mixing of the boundary layer flow, and in some instances, iii) PM_{10} loss of feldspar or salt (e.g. uncrusted surfaces).

Under daytime conditions, mass losses during each 30 minute wind tunnel run ranged from 0.0 g for crust surfaces M3[1,8]$_C$, H3[15]$_C$, T1[35]$_C$ and H1[26.4]$_C$ to 65.2 g for the uncrusted playa sediment (P4$_C$). Of the degraded crusts, T3[35]$_C$ lost the greatest mass (18.7 g) and showed visible scour marks on the post-wind-tunnel scan (Figure 12a, e and i). Although M3[3.3,21.1]$_C$ lost 6.2 g during the wind tunnel run, this is believed to have resulted entirely from evaporation. Efflorescence and crystal development were detected by laser scanning around the edges of salt crystals that were already present (either as new crystals or growth of original crystals; Figure 12f), while the elevation ratio for the M3[3.3,21.1]$_C$ crust (0.006) indicates greater surface expansion than erosion. A similar argument can be made for P3$_C$, and to a lesser extent (mass loss < 1 g) for P2$_C$, W2$_C$, M2[3.3,21.1]$_C$, M3[7,21.1]$_C$, M3[2,12]$_C$, T1[35]$_C$ and H1[26.4]$_C$. However when the crusted surfaces were fractured (environmental condition D), increases in the mass loss and the elevation ratios were observed during wind tunnel testing for a majority of crust types, except for H3[26.4]$_D$, M3[3.3,21.1]$_D$ and P3$_D$. This increased mass loss on observed from disturbed crusts agrees with field tunnel findings where measured sediment flux increased after several cattle disturbances (Baddock *et al.*, 2011). Mass loss on our continuous crusts was less than that for their degraded or spray crust counterparts, unless the continuous crusts were disturbed (Figure 9c).

Additionally, in our experiments undisturbed crust thickness was less important in determining the actual mass lost (combined sediment and water; correlation coefficient -0.5; Figure 10b), but thinner crusts produced more mass loss after they had been disturbed (correlation coefficient -0.46; Figure 10d). This agrees with the elevation ratio findings, that undisturbed crust thickness was less important for determining surface deformation rates (correlation coefficient -0.36), but that crust thickness may influence the reworking of the crust after it has been disturbed, with thinner crusts depicting more erosion (correlation coefficient -0.59).

Although the experiments reported in this study excluded the direct influence of solar radiation on surface dynamics and heat exchange, and did not seek to examine crystal habit or mineralogy specifically, they provide insight into the relative emissivity of various crusts types formed under identical climate conditions, as characterized by diurnal fluctuations in temperature and humidity on the Sua Pan in winter. The results from this study suggest that the crust state (i.e. the continuum between continuous or degraded) for natural surfaces may not be as important as the salt chemistry; which is consistent with other in-situ playa studies where efflorescence potential (Cahill *et al.,* 1996) and crystal habit (Buck *et al.,* 2011) have been key indicators of dust flux. Salt concentration and crust development time are also important factors which influence the threshold response of undisturbed and disturbed crusts (e.g. Nickling and Ecclestone, 1981; Reynolds et al., 2007). The crust samples prepared using stronger salt concentrations experienced more sub-efflorescence and surface-efflorescence during the development phase and so it is possible that the lower u_{*t} observed for high salt concentration disturbed crusts (Figure 9b) resulted from an increased availability of low density, salty, 'fluffy' sediment beneath the crust which could be entrained once their crust had been disturbed, but which was supressed while the initial crust was intact. Field studies have also found inconsistencies between salt concentration and dust emission potential (King et al, 2011), and more research is needed to look specifically at in situ geochemistry as dust is emitted (Buck et al., 2011).

4. Conclusions

The exploratory laboratory experiments reported in this paper address dust emission potential from degraded and continuous evaporative salt crusts under varying climatic conditions. The results demonstrate considerable complexity in the relationships between the flux of dust emitted from a playa surface to the atmospheric boundary layer, the threshold wind speed required for this to happen, and the physicochemical characteristics of the surface, specifically the type and form of the salt crust. Crusts formed from Na_2SO_4 and degraded crust types are typically more emissive than continuous NaCl crusts during hot, dry conditions typical of daytime in deserts. The results from this study further demonstrate that emission from salt crusts is unlikely to occur under night time conditions when the humidity is relatively high and temperature low. In general, we find that disturbed crusts may become emissive at wind speeds that are as much as 50% lower than for their undisturbed counterparts, while on average disturbed crusts may emit 52% more dust. As a coarse approximation, PM_{10} fluxes from a variety of undisturbed salt crusts are found to be in the order of 10^{-1}, as compared to 100 $\mu g/m^2/s^1$ for uncemented silts and clays. These values are relatively low as compared to those published for surfaces containing sand particles. They strongly reflect the isolated role of aerodynamic entrainment in dust emission, in the absence of saltators which are highly efficient in splashing fine grains out of the bed surface upon their impact. It is further speculated that a substantial fraction of the dust emitted is actually comprised of salt crystals rather than sedimentary particles, especially for playa surfaces that actively effloresce with little restriction on evaporation. Whilst degraded crusts with weak salt concentrations are typically more emissive than crusts that are undisturbed, crusts with a higher salt concentration will exhibit a lower u_{*t} after disturbance.

In future laboratory experiments, we recommend the use of evaporative crusts typical of salt pans, as compared to conventional treatments in which crusts have been created by spraying saline water directly onto the surface (e.g. Treatment 1), since the dust emission threshold for disturbed crusts can be underestimated by as much as 63%. Effort should be focused solely upon emissions measurement under hot, dry daytime conditions, as these were the only environmental conditions for which elevated dust concentrations were observed. This paper reports some of the first experimental data to support the parameterization and improved performance of spatially distributed dust emission models in their application to vast areas for which almost no field measurements exist

Acknowledgements

Grants from NSERC (Discovery) and CFI (Microenvironments Labs) support the research program of McKenna Neuman and the Trent Environmental Wind Tunnel (TEWT). Travel for Nield was funded by a Royal Society International Exchange Grant (IE130835). Collection of salt pan samples and field data from Botswana was enabled as part of the DO4models project (NERC NE/H021841/1; World University Network; University of Southampton SIRDF; Botswana Ministry of Environment, Wildlife, and Tourism permit EWT 8/36/4 XIV), with field collaborators J King, FD Eckardt, K Vickery, DSG Thomas and R Washington and local support and site access from Botswana Ash (pty) Ltd. WG Nickling is thanked for insights on making wind tunnel evaporative salt crusts and D Ogungbemide for assisting with grain size analysis. Editors, reviewers, J King and T Gill are thanked for comments which helped to focus and improve this manuscript.

References

Baddock MC, Ginoux P, Bullard JE, Gill TE. 2016. Do MODIS-defined dust sources have a geomorphological signature?: *Geophysical Research Letters*, 43: 2606–2613.

Baddock MC, Zobeck TM, Van Pelt RS, Fredrickson EL. 2011. Dust emissions from undisturbed and disturbed, crusted playa surfaces: Cattle trampling effects: *Aeolian Research*, **3**: 31-41.

Baddock MC, Bullard JE, Bryant RG. 2009. Dust source identification using MODIS: A comparison of techniques applied to the Lake Eyre Basin, Australia: *Remote Sensing of Environment*, **113**: 1511-1528.

Benavente D, Brimblecombe P, Grossi CM. 2015. Thermodynamic calculations for the salt crystallisation damage in porous built heritage using PHREEQC: *Environmental Earth Sciences*, **74**: 2297-2313.

Bryant RG, Sellwood BW, Millington AC, Drake NA. 1994. Marine-Like Potash Evaporite Formation on A Continental Playa - Case-Study from Chott-El-Djerid, Southern Tunisia: *Sedimentary Geology*, **90**: 269-291.

Bryant RG, Bigg GR, Mahowald NM, Eckardt FD, Ross SG. 2007. Dust emission response to climate in southern Africa: *Journal of Geophysical Research-Atmospheres*, **112**: D09207.

Bryant RG. 2013. Recent advances in our understanding of dust source emission processes: *Progress in Physical Geography*, **37**: 397-421.

Buck BJ, King J, Etyemezian V. 2011. Effects of Salt Mineralogy on Dust Emissions, Salton Sea, California: *Soil Science Society of America Journal*, **75**: 1971-1985.

Bullard JE, Harrison SP, Baddock MC, Drake N, Gill TE, McTainsh G, Sun Y. 2011. Preferential dust sources: A geomorphological classification designed for use in global dust-cycle models: *Journal of Geophysical Research: Planets*, **116**: F04034.

Cahill TA, Gill TE, Reid JS, Gearhart EA, Gillette DA. 1996. Saltating particles, playa crusts and dust aerosols at Owens (dry) Lake, California: *Earth Surface Processes and Landforms*, **21**: 621-639.

Eckardt FD, Bryant RG, McCulloch G, Spiro B, Wood WW. 2008. The hydrochemistry of a semi-arid pan basin case study: Sua Pan, Makgadikgadi, Botswana: *Applied Geochemistry*, **23**: 1563-1580.

Eloukabi H, Sghaier N, Ben Nasrallah S, Prat M. 2013. Experimental study of the effect of sodium chloride on drying of porous media: The crusty-patchy efflorescence transition: *International Journal of Heat and Mass Transfer*, **56**: 80-93.

Espinosa-Marzal RM, Scherer GW. 2010. Advances in Understanding Damage by Salt Crystallization: *Accounts of Chemical Research*, **43**: 897-905.

Genkinger S, Putnis A. 2007. Crystallisation of sodium sulfate: supersaturation and metastable phases: *Environmental Geology*, **52**: 295-303.

Gill TE. 1996. Eolian sediment generated by anthropogenic disturbance of playas: human impacts on th egeomorphic system and geomorphic impacts on the human system: *Geomorphology*, **17**: 207-228.

Gillette D, Ono D, Richmond K. 2004. A combined modeling and measurement technique for estimating windblown dust emissions at Owens (dry) Lake, California: *Journal of Geophysical Research-Earth Surface*, **109**.

Gillette DA, Niemeyer TC, Helm PJ. 2001. Supply-limited horizontal sand drift at an ephemerally crusted, unvegetated saline playa: *Journal of Geophysical Research-Atmospheres*, **106**: 18085-18098.

Groeneveld DP, Huntington JL, Barz DD. 2010. Floating brine crusts, reduction of evaporation and possible replacement of fresh water to control dust from Owens Lake bed, California: *Journal of Hydrology*, **392**: 211-218.

Hahnenberger M, Nicoll K. 2014. Geomorphic and land cover identification of dust sources in th eeaster Great Basin of Utah, U.S.A.: *Geomorphology*, **204**: 657-672.

Haustein K, Washington R, King J, Wiggs G, Thomas DSG, Eckardt FD, Bryant RG, Menut L. 2015. Testing the performance of state-of-the-art dust emission schemes using DO4Models field data: *Geosci.Model Dev.*, **8**: 341-362.

Houser CA, Nickling WG. 2001. The factors influencing the abrasion efficiency of saltating grains on a clay-crusted playa: *Earth Surface Processes and Landforms*, **26**: 491-505.

Kempf SK, Tyler SW. 2006. Spatial characterization of land surface energy fluxes and uncertainty estimation at the Salar de Atacama, Northern Chile: *Advances in Water Resources*, **29**: 336-354.

King J, Etyemezian V, Sweeney M, Buck BJ, Nikolich G. 2011. Dust emission variability at the Salton Sea, California, USA: *Aeolian Research*, **3**: 67-79.

Kracek FC. 1928. International Critical Tables 3, *in* Washburn E.W., ed., New York, McGraw Hill.

Langbein WB. 1961. Salinity and hydrology of closed lakes: *U.S. Geological Survey Professional Paper*, **412**: 1-20.

Langston G, McKenna Neuman C. 2005. An experimental study on the susceptibility of crusted surfaces to wind erosion: A comparison of the strength properties of biotic and salt crusts: *Geomorphology*, **72**: 40-53.

Macpherson T, Nickling WG, Gillies JA, Etyemezian V. 2008. Dust emissions from undisturbed and disturbed supply-limited desert surfaces: *Journal of Geophysical Research*, **113**: F02S04, doi:10.1029/2007JF000800.

Mahowald NM, Bryant RG, del Corral J, Steinberger L. 2003. Ephemeral lakes and desert dust sources: *Geophysical Research Letters*, **30**: 46-1-46-4.

McKenna Neuman C. 1998. Particle transport and adjustments of the boundary layer over rough surfaces with an unrestricted, upwind supply of sediment: *Geomorphology*, **25**: 1-17.

McKenna Neuman C. 2003. Effects of temperature and humidity upon the entrainment of sedimentary particles by wind: *Boundary-Layer Meteorology*, **108**: 61-89.

McKenna Neuman C. 2004. Effects of temperature and humidity upon the transport of sedimentary particles by wind: *Sedimentology*, **51**: 1-17.

Mees F, Castaneda C, Herrero J, Van Ranst E. 2011. Bloedite sedimentation in a seasonally dry saline lake (Salada Mediana, Spain): *Sedimentary Geology*, **238**: 106-115.

Nachshon U, Shahraeeni E, Or D, Dragila M, Weisbrod N. 2011a. Infrared thermography of evaporative fluxes and dynamics of salt deposition on heterogeneous porous surfaces: *Water Resources Research*, **47**.

Nachshon U, Weisbrod N, Dragila MI, Grader A. 2011b. Combined evaporation and salt precipitation in homogeneous and heterogeneous porous media: *Water Resources Research*, **47**.

Nickling WG, Ecclestone M. 1981. The effects of soluble salts on the threshold shear velocity of fine sand: *Sedimentology*, **28**: 505-510.

Nickling WG, McKenna Neuman C. 1997. Wind tunnel evaluation of a wedge-shaped aeolian transport trap: *Geomorphology*, **18**: 333-345.

Nickling WG. 1984. The stabilizing role of bonding agents on the entrainment of sediment by wind: *Sedimentology*, **31**: 111-117.

Nield JM, Bryant RG, Wiggs GFS, King J, Thomas DSG, Eckardt FD, Washington R. 2015. The dynamism of salt crust patterns on playas: *Geology*, **43**: 31-34.

Nield JM, Wiggs GFS, King J, Bryant RG, Eckardt FD, Thomas DSG, Washington R. 2016. Climate-surface-pore-water interactions on a salt crusted playa: implications for crust pattern and surface roughness development using terrestrial laser scanning: *Earth Surface Processes and Landforms*, **41**: 738-753.

Nield JM, King J, Wiggs GFS, Leyland J, Bryant RG, Chiverrell RC, Darby SE, Eckardt FD, Thomas DSG, Vircavs LH, Washington R. 2013. Estimating aerodynamic roughness over complex surface terrain: *Journal of Geophysical Research: Atmospheres*, **118**: 2013JD020632.

O'Brien P, McKenna Neuman C. 2012. A wind tunnel study of particle kinematics during crust rupture and erosion: *Geomorphology*, **173-174**: 149-160.

Prospero JM, Ginoux P, Torres O, Nicholson SE, Gill TE. 2002. Environmental characterization of global sources of atmospheric soil dust identified with the Nimbus 7 Total Ozone Mapping Spectrometer (TOMS) absorbing aerosol product: *Reviews of Geophysics*, **40**: 2-1-2-31.

Rad MN, Shokri N, Sahimi M. 2013. Pore-scale dynamics of salt precipitation in drying porous media: *Physical Review e*, **88**.

Reynolds RL, Yount JC, Reheis M, Goldstein H, Chavez P, Fulton R, Whitney J, Fuller C, Forester RM. 2007. Dust emission from wet and dry playas in the Mojave desert, USA: *Earth Surface Processes and Landforms*, **32**: 1811-1827.

Rodriguez-Navarro C, Doehne E. 1999. Salt weathering: Influence of evaporation rate, supersaturation and crystallization pattern: *Earth Surface Processes and Landforms*, **24**: 191-209.

Rodriguez-Navarro C, Doehne E, Sebastian E. 2000. How does sodium sulfate crystallize? Implications for the decay and testing of building materials: *Cement and Concrete Research*, **30**: 1527-1534.

Rosen MR. 1994. The importance of groundwater in playas: a review of playa classifications and the sedimentology and hydrology of playas, *in* Rosen, M.R., ed., *Paleoclimate and Basin Evolution of Playa Systems, Geological Society of America Special Paper 289*: Boulder, CO, Geological Society of America, 1-18.

Saint-Amand P, Mathews LA, Gaines C, Reinking R. 1986. Dust storms from Owens and Mono Valleys, California, China Lake, CA, Naval Weapons Center Technical Publication Series 6731.

Sanderson S, McKenna Neuman C, Boulton JW. 2014. Windblown fugitive dust emissions from smelter slag: *Aeolian Research*, **13**: 19-29.

Shahidzadeh-Bonn N, Desarnaud J, Bertrand F, Chateau X, Bonn D. 2010. Damage in porous media due to salt crystallization: *Physical Review e*, **81**.

Steiger M, Asmussen S. 2008. Crystallization of sodium sulfate phases in porous materials: The phase diagram Na2SO4-H2O and the generation of stress: *Geochimica et Cosmochimica Acta*, **72**: 4291-4306.

Sweeney MR, McDonald EV, Etyemezian V. 2011. Quantifying dust emissions from desert landforms, eastern Mojave Desert, USA: *Geomorphology*, **135**: 21-34.

Sweeney MR, Zlotnik VA, Joeckel RM, Stout JE. 2016. Geomorphic and hydrologic controls of dust emissions during drought from Yellow Lake playa, West Texas, USA: *Journal of Arid Environments*, **133**: 37-46.

Thaulow N, Sahu S. 2004. Mechanism of concrete deterioration due to salt crystallization: *Materials Characterization*, **53**: 123-127.

Tollerud HJ, Fantle MS. 2014. The temporal variability of centimeter-scale surface roughness in a playa dust source: synthetic aperture radar investigation of playa surface dynamics: *Remote Sensing of the Environment*, **154**: 285-297.

Tsui N, Flatt RJ, Scherer GW. 2003. Crystallization damage by sodium sulfate: *Journal of Cultural Heritage*, **4**: 109-115.

Tyler SW, Kranz S, Parlange MB, Albertson J, Katul GG, Cochran GF, Lyles BA, Holder G. 1997. Estimation of groundwater evaporation and salt flux from Owens lake, California, USA: *Journal of Hydrology*, **200**: 110-135.

Vickery, K.J., 2014, A case study on dust supply from the Makgadikgadi Pans, Botswana [Doctor of Philosophy : University of Cape Town.

Viles HA, Goudie AS. 2007. Rapid salt weathering in the coastal Namib desert: Implications for landscape development: *Geomorphology*, **85**: 49-62.

Washington R, Todd M, Middleton NJ, Goudie AS. 2003. Dust-storm source areas determined by the total ozone monitoring spectrometer and surface observations: *Annals of the Association of American Geographers*, **93**: 297-313.

Washington R, Todd MC, Lizcano G, Tegen I, Flamant C, Koren I, Ginoux P, Engelstaedter S, Bristow CS, Zender CS, Goudie AS, Warren A, Prospero JM. 2006. Links between topography, wind, deflation, lakes and dust: The case of the Bodele Depression, Chad: *Geophysical Research Letters*, **33**: L09401.

Webb NP, Strong CL. 2011. Soil erodibility dynamics and its representation for wind erosion and dust emission models: *Aeolian Research*, **3**: 165-179.

White BR, Mounla H. 1991. An experimental study of Froude Number effect on wind-tunnel saltation: *Acta Mechanica Supplementum*, **1**: 145-157.

Zender CS, Kwon EY. 2005. Regional contrasts in dust emission responses to climate: *Journal of Geophysical Research-Atmospheres*, **110**: D13201.

Tables

Table 1 Salt concentrations and methods used to develop crust samples. Letters denote sediment salt preparation type (P-Playa, T- Na_2SO_4, H- NaCl, W-Water, M-mixed salt). Numbers indicate crust preparation type (spray = 1, continuous = 2, degraded = 3, uncrusted = 4). Square brackets denote salt concentrations (sulphate first, chloride second). All samples were tested in the wind tunnel under environmental condition C (hot). Subscripts denote testing under additional wind tunnel environmental conditions (A = cool, B = warm, D = disturbed).

Description	Na_2SO_4 (w%)	NaCl (w%)	Spray Treatment 1	Continuous (saturation) Treatment 2	Degraded Treatment 3	Un-crusted
Playa sediment (Sua Pan)	-	-	-	$P2_{ABD}$	$P3_{ABD}$	P4
Na_2SO_4 (high)	35	-	T1[35]		T3[35]	
Na_2SO_4 (low)	16.5	-			$T3[16.5]_{ABD}$	
NaCl (high)	-	26.4	$H1[26.4]_D$		$H3[26.4]_D$	
NaCl (low)	-	15			$H3[15]_{ABD}$	
Mixed salt (high)	7	21.1	$M1[7,21.1]_D$	$M2[7,21.1]_{ABD}$	$M3[7,21.1]_D$	M4[7,21.1]
Mixed salt (low 1)	3.3	21.1		$M2[3.3,21.1]_D$	$M3[3.3,21.1]_D$	
Mixed salt (low 2)	2	12			$M3[2,12]_{ABD}$	
Mixed salt (low 3)	1	8			M3[1,8]	
Mixed salt (low 4)	0.5	4			$M3[0.5,4]_D$	
Water	-	-	W1	W2	$W3_D$	$W4_{AB}$

Table 2 Parameters for vertical dust flux (F, Equation 3) relations with shear velocity, as measured over each wind tunnel run for environmental conditions C (upper row) and D (lower row). Only samples with regression coefficient (R^2) greater than 0.5 and p-value less than 0.01 are reported.

Description	Spray (Treatment 1)				Continuous (Treatment 2)				Degraded (Treatment 3)				Un crusted (Treatment 4)			
	R^2	a	b	u_{*t} m/s	R^2	a	b	u_{*t} m/s	R^2	a	b	u_{*t} m/s	R^2	a	b	u_{*t} m/s
Playa sediment (P; Sua Pan)					0.94	$2.4x10^{-4}$	7	0.35				0.40	0.96	$9.8x10^{-4}$	6	0.25
					0.87	$3.3x10^{-4}$	1	0.52				0.51				
Na_2SO_4 (T[35]; high)	0.76	$1.7x10^{-4}$	2	0.30					0.90	$3.2x10^{-4}$	7	0.25				
Na_2SO_4 (T[16.5]; low)												0.39				
									0.53	$2.2x10^{-4}$	2	0.34				
NaCl (H[26.4]; high)				0.36					0.72	$2.9x10^{-4}$	3	0.54				
				0.33					0.53	$8.0x10^{-5}$	1	0.31				
NaCl (H[15]; low)									0.77	$3.9x10^{-4}$	2	0.55				
												0.40				
Mixed salt (M[7,21.1])	0.63	$3.1x10^{-4}$	1	0.41				0.55				0.51	0.95	$2.4x10^{-4}$	6	0.28
				0.20				0.55	0.88	$2.1x10^{-4}$	2	0.27				
Mixed salt (M[3.3,21.1])								0.49								
								0.50								
Mixed salt (M[2,12])									0.97	$1.1x10^{-3}$	2	0.55				
												0.37				
Mixed salt (M[1,8])												0.41				
												0.40				
Mixed salt (M[0.5,4])									0.65	$4.5x10^{-4}$	5	0.36				
									0.82	$5.0x10^{-5}$	5	0.23				
Water (W)	0.85	$5.8x10^{-4}$	4	0.38				0.50	0.94	$2.7x10^{-4}$	8	0.37	0.97	$1.2x10^{-4}$	9	0.28
									0.96	$5.0x10^{-5}$	7	0.23				

Figures

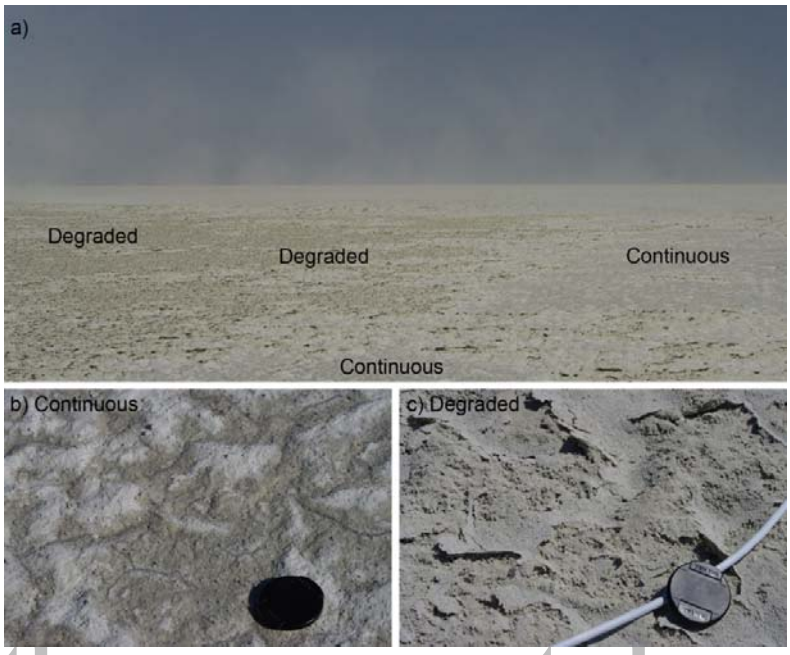

Figure 1 a) Dust emission from a mixed degraded and continuous surface on Sua Pan, Botswana, August 2012. Enlargements of surface texture on a b) continuous and c) degraded Sua Pan surface, August 2011. Lens cap for scale (diameter = 60 mm).

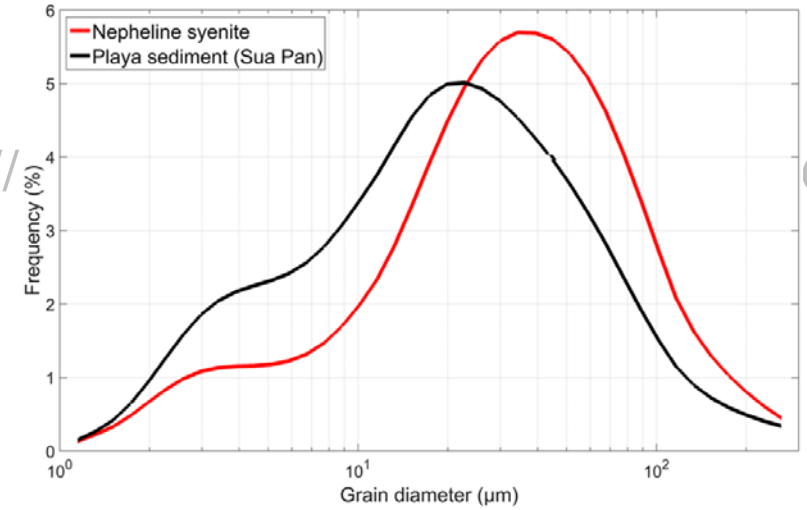

Figure 2 Particle size distributions for typical Sua Pan and nepheline syenite sediment used to construct the test surfaces.

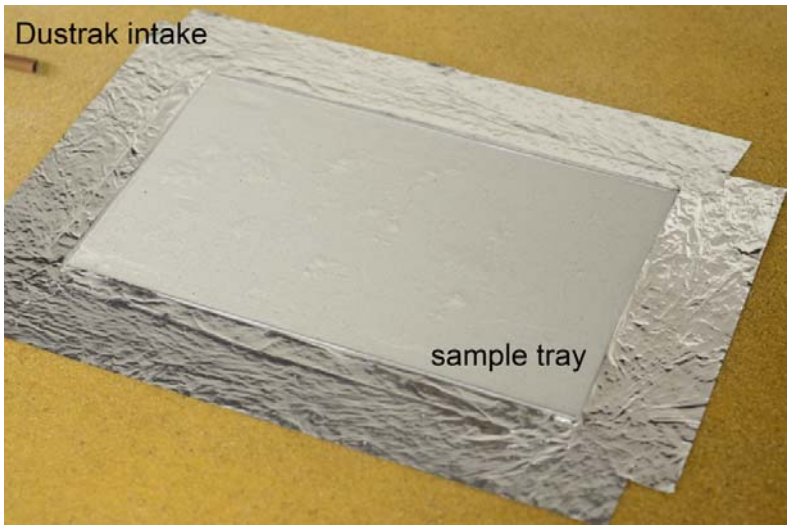

Figure 3 Typical set-up in the wind tunnel, with the sample tray inset so that the crust was level with the tunnel floor and sealed with tape. The intake tube for the DustTrak is shown immediately downwind of the test surface and is aligned parallel to the approaching air flow.

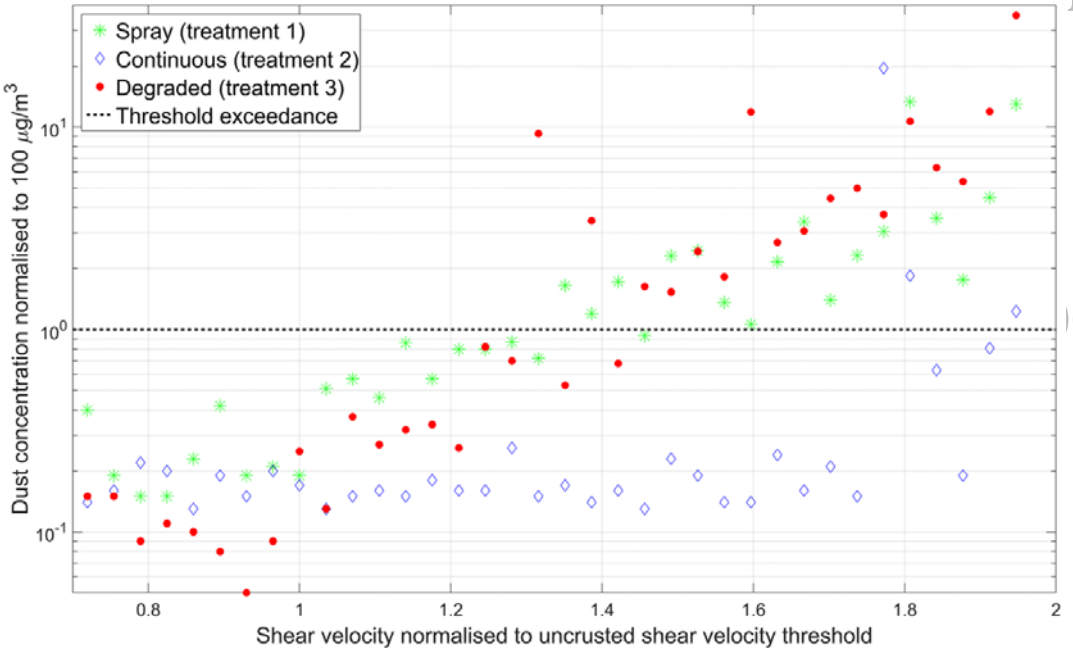

Figure 4 Dust concentration values for reference wind tunnel experiments ($W1_C$, $W2_C$ and $W3_C$) in which the feldspar particles were wetted with deionized water using various treatment techniques.

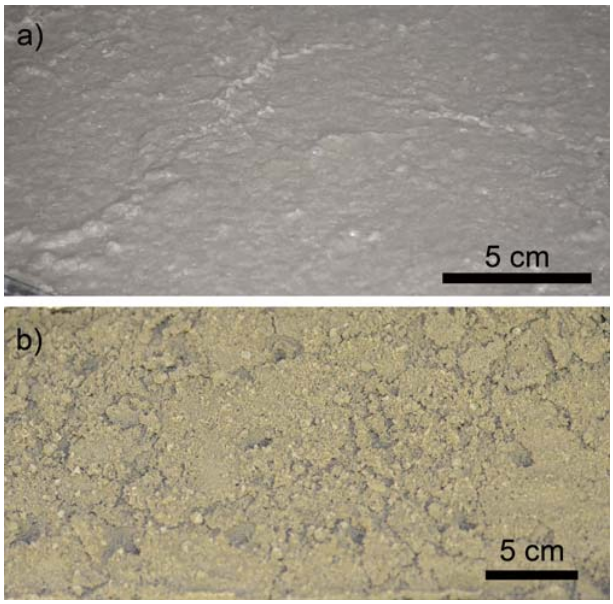

Figure 5 Examples of a) continuous ($P2_C$) and b) disturbed degraded ($P3_D$) crusts prepared in the climate controlled laboratory using Sua Pan sediments.

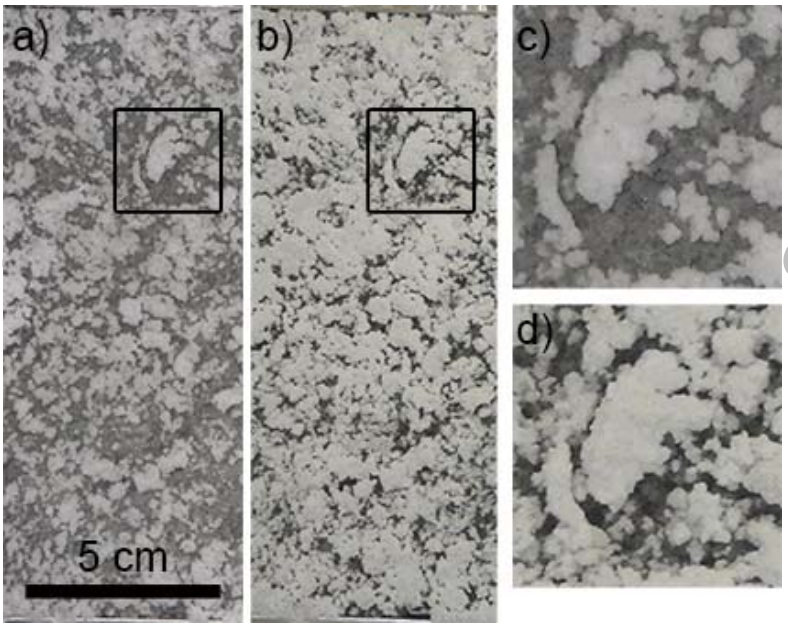

Figure 6 Photos of the surface of T3[16.5] showing crystal growth over time with a) representing cool night time conditions (11°C and relative humidity 60%) as compared to b) for warm daytime conditions (25°C and relative humidity 30%). Images c) and d) are enlargements of the areas within the black boxes shown in a) and b), respectively. The scale is the same for images a and b.

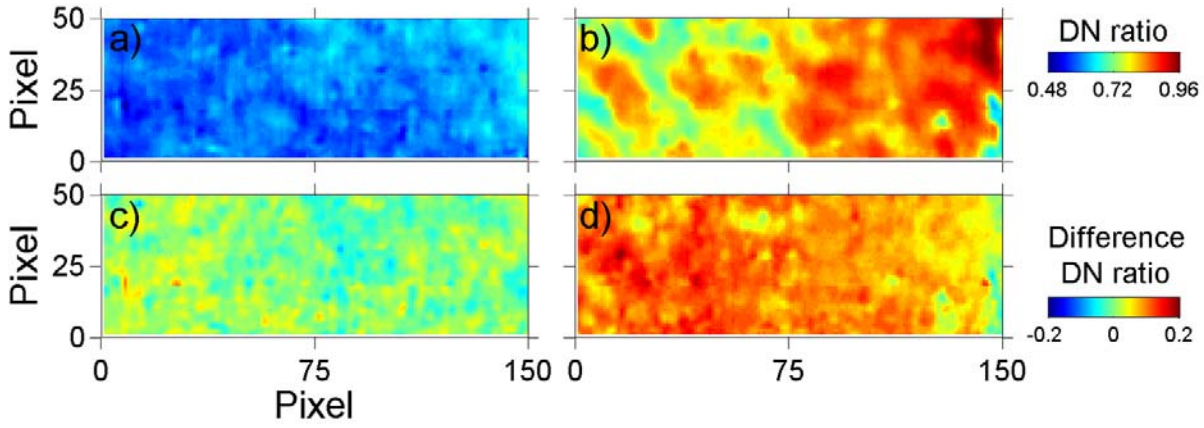

Figure 7 Infrared camera DN values for the degraded Na_2SO_4 crust T3[16.5] during the crust development phase. Axis values are given in pixels. DN ratio for a) the start of a cool phase (11°C, relative humidity 60%), as compared to b) the end of the subsequent hot phase (25°C, relative humidity 30%). Colours trending to red indicate high salt content and low moisture, as compared to blue representing low salt content and high moisture. The difference values quantify the absolute change in the DN ratio between the beginning and end of each climate period, for conditions c) cool and d) hot.

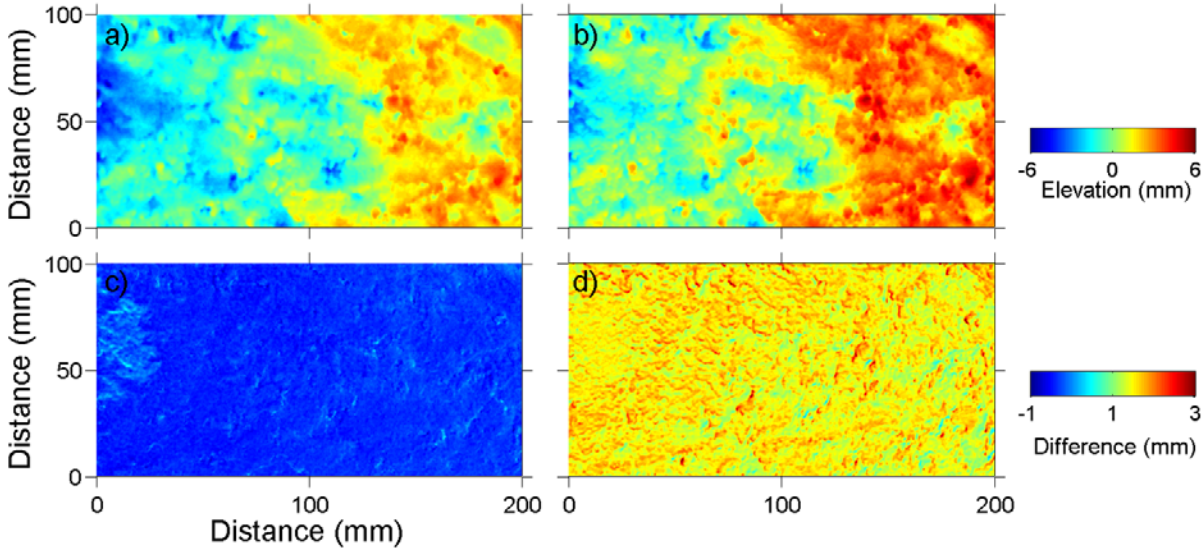

Figure 8 Variation in elevation within the degraded Na_2SO_4 crust T3[16.5] during the crust development phase. These DEMs match the time of capture for the DN data shown in Figure 7. Colours in the top row indicate the relative surface elevation (e.g. dark red pixels represent elevations lying 6 mm above the mean for the entire surface, and dark blue pixels, 6 mm below). Image a) represents the start of a cool period (11°C, relative humidity 60%), as compared to b) which characterizes the end of the subsequent hot period (25°C, relative humidity 30%). The difference values quantify the absolute change in surface elevation between the beginning and end of each climate period, for conditions c) cool and d) hot.

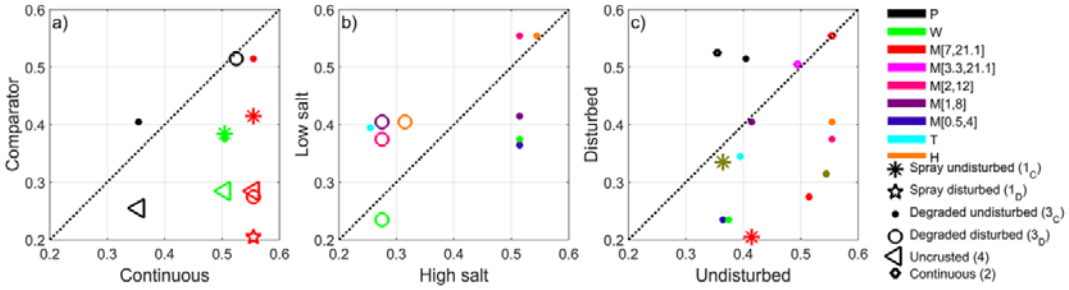

Figure 9 Comparison of u^*_t (m/s) among various experiments: a) continuous versus other crust types, b) high versus low salt concentration (degraded crusts only), and c) undisturbed versus disturbed crusts. Values falling directly on the diagonal 1:1 line indicate that the treatment has no effect on the threshold shear velocity for PM_{10} emission. Varied symbols distinguish the physical properties of the crust, and colours the chemical properties (see Table 1 for a full description of the nomenclature). All experiments were conducted at 25 °C.

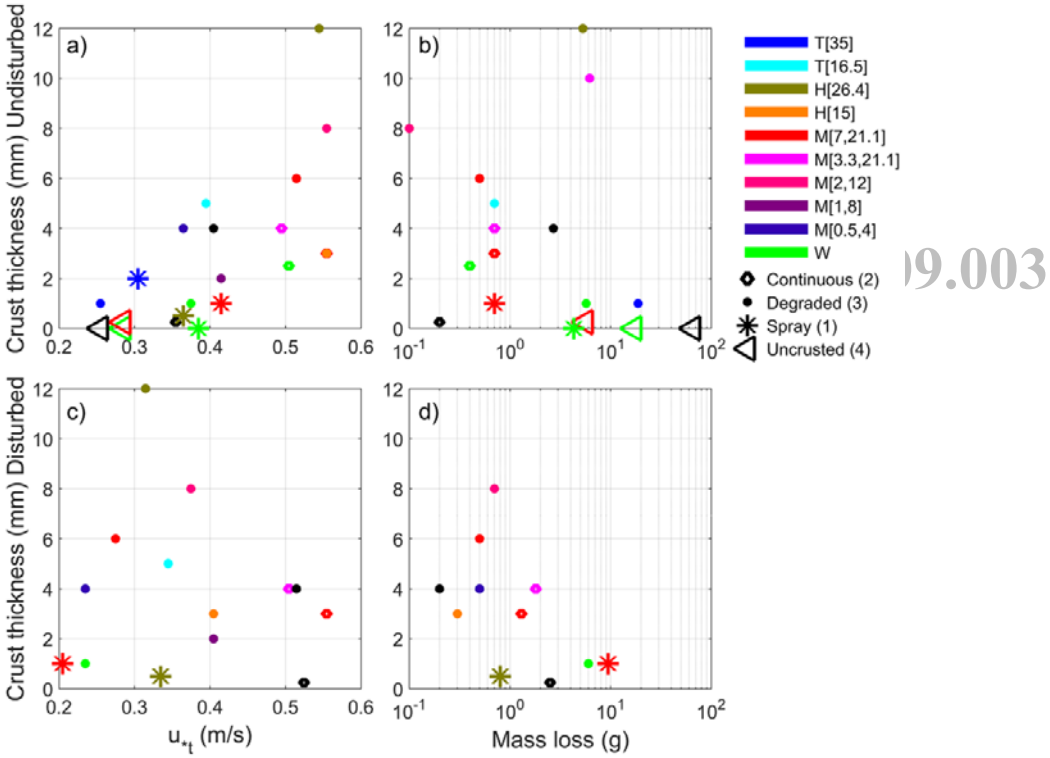

Figure 10 Relationship between crust thickness and two sediment transport indicators: the threshold shear velocity for dust emission (plots a and c), and the total mass loss (plots b and d). The top row refers to undisturbed crusts and the bottom row to disturbed crusts. Varied symbols distinguish the physical properties of the crust, and colours the chemical properties (see Table 1 for a full description of the nomenclature). All experiments were conducted at 25 °C.

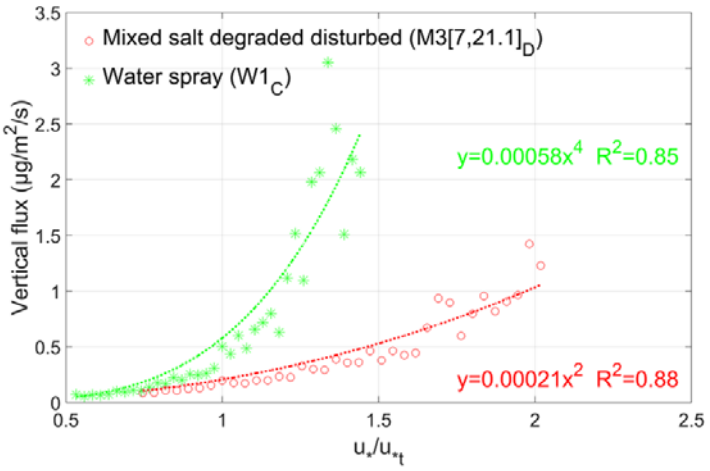

Figure 11 Selected examples of the relationship between the normalized shear velocity and the vertical dust flux.

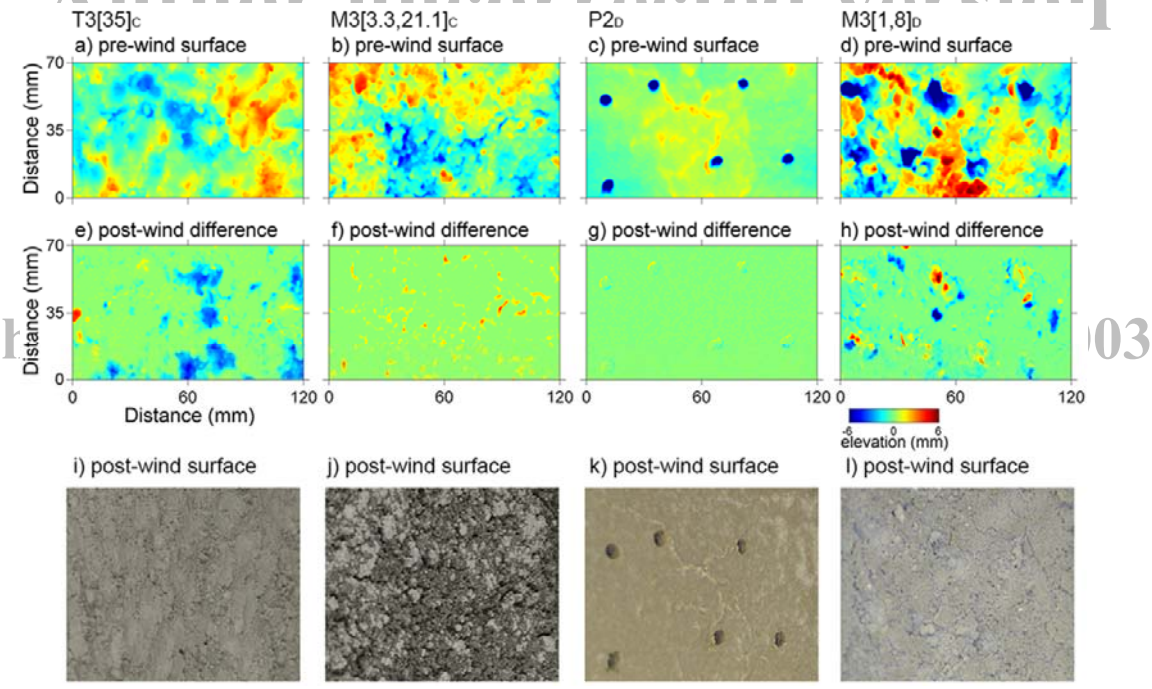

Figure 12 Plots (a-h) provide DEMs of selected crust sections. The plots in the top row refer to the crust surface before each wind tunnel experiment. Colours indicate the surface elevation above (red) and below (blue) the mean elevation. The centre row of plots show the difference in crust elevation arising from exposure to wind, with the airflow direction oriented from bottom to top. Photos (i-l) were captured after the wind tunnel experiments, with the image area corresponding approximately to that which was scanned. Plots in the two columns on the left refer to environmental condition C, and the remaining two on the right to environmental condition D (e.g. where surface punctures are clearly evident).